CrossMark

Composition dependence of phase structure and piezoelectric properties in $(0.98-x)(K_{0.4}Na_{0.6})NbO_3$–$0.02CaZrO_3$–$xBi_{0.5}Na_{0.5}HfO_3$ ternary ceramics

Dandan Xue[1] · Yunyi Liu[1] · Meng Shi[1] · Pei Wang[1] · Leiyang Zhang[1] · Gang Liu[1] · Zhiqian Chen[1] · Yi Chen[1]

Abstract Lead-free perovskite $(0.98-x)(K_{0.4}Na_{0.6})NbO_3$–$0.02CaZrO_3$–$xBi_{0.5}Na_{0.5}HfO_3$ (KNN–CZ–xBNH) ceramics were prepared by a conventional solid-state reaction method, and the connections between their composition, phase structure, and electrical properties were investigated. The X-ray diffraction results, together with the temperature dependence of dielectric properties, showed that a rhombohedral–tetragonal (R–T) phase boundary was successfully constructed in the composition range of $0.04 \leq x \leq 0.045$. An enhancing effect of R–T phase boundary on the piezoelectric activity was observed, and the ceramics with the composition $x = 0.045$ exhibited the highest piezoelectric properties, possessing a piezoelectric constant d_{33} of 320 pC/N and a planar electromechanical coupling coefficient of 0.40. In addition, it was found that while adding a small amount of $Bi_{0.5}Na_{0.5}HfO_3$ could result in very large grain sizes in the $(K,Na)NbO_3$-based ceramics, adding too much of it would lead to extremely fine grain sizes. In general, our experimental results indicate that the KNN–CZ–xBNH ceramics are promising candidate materials for lead-free piezoelectric applications.

1 Introduction

$Pb(Zr,Ti)O_3$ (PZT)-based ceramics have been widely applied in many fields, such as sensors, actuators, transducers, etc., due to their excellent electrical properties and relatively high Curie temperature (T_C) [1, 2]. However,

unfortunately, lead existed in PZT-based ceramics can cause serious harm to the health of both the environment and humans during their production, usage, and disposal operations, owing to the high toxicity of lead. Therefore, considerable attention has been paid to lead-free piezoelectric materials for their replacement of PZT-based ceramics [3–5], especially after the implementation of the RoHS legislation in July 2006 in Europe [6], which forbids the use of lead in electronic products. Among all lead-free materials researched so far, the $(K,Na)NbO_3$ (KNN)-based ceramics possess relatively high values of both piezoelectric activity and Curie temperature [7–9], and therefore have attracted increasing attention around the world, particularly after the breakthrough made by Saito et al. in 2004 [10], when a great improvement was achieved in the piezoelectric properties of KNN-based materials, by using the reactive-templated grain growth method.

However, generally speaking, the piezoelectric properties of pure KNN ceramics are poor when compared to commercial PZT-based ceramics [11–13], presenting a major limitation for their practical applications. Therefore, in order to improve their piezoelectric activities, many researchers have focused on the construction of phase boundaries in KNN-based ceramics [14–22], as they can provide more spontaneous polarization directions [1], thus leading to better piezoelectric properties. It is well-known that pure KNN undergoes a rhombohedral–orthorhombic (R–O) phase transition at − 123 °C, and an orthorhombic–tetragonal (O–T) phase transition at 210 °C [7]. And the phase boundaries, including R–O, O–T, and rhombohedral–tetragonal (R–T) phase boundaries, are generally formed by means of shifting the temperatures of R–O and/or O–T phase transitions (namely, the $T_{R–O}$ and/or $T_{O–T}$) to near room temperature, with the introduction of different additives [7, 14–22].

✉ Yi Chen
mrchenyi@swu.edu.cn

1 Faculty of Materials and Energy, Southwest University, Chongqing 400715, People's Republic of China

It is the R–T phase boundary that has been receiving more and more attention in recent years [23–25], since it can allow for piezoelectric properties comparable to those of certain commercial PZT-based ceramics. The construction of the R–T phase boundary requires that the T_{R-O} and T_{O-T} merge at room temperature. Some additives, such as $AZrO_3$ (A = Ba, Sr, and Ca) and $Bi_{0.5}Na_{0.5}ZrO_3$, play an important role in the formation of R–T phase boundaries, as they can simultaneously shift both the two temperatures to room temperature [19, 21, 22]. Very recently, some authors found that the $Bi_{0.5}Na_{0.5}HfO_3$ (BNH) had similar effects on the two temperatures as $AZrO_3$ and $Bi_{0.5}Na_{0.5}ZrO_3$, and hence could bring about significant improvement in the piezoelectric properties of KNN-based ceramics [26–28].

Therefore, in the present work, the $CaZrO_3$ and BNH co-modified KNN-based ceramics, with the general chemical formula of $(0.98 - x)(K_{0.4}Na_{0.6})NbO_3-0.02CaZrO_3-xBi_{0.5}Na_{0.5}HfO_3$ (abbreviated as KNN–CZ–xBNH), were projected and fabricated by a conventional solid-state reaction method. A study was carried out to assess the influences of BNH content on the phase structure, microstructure, and piezoelectric properties of the ceramics. It was found that the ceramics possessed an R–T phase boundary in the composition range of $0.04 \leq x \leq 0.045$, near which an enhanced piezoelectric activity was achieved.

2 Experimental procedure

The KNN–CZ–xBNH ceramics were prepared by a conventional solid-state reaction from adequate mixtures of K_2CO_3 (99%), Na_2CO_3 (99.8%), Nb_2O_5 (99.5%), $CaCO_3$ (99%), ZrO_2 (99%), Bi_2O_3 (99%), and HfO_2 (99.99%) powders. All the raw materials were weighed in the stoichiometric amounts, and then were ball-milled in ethanol with agate media for 24 h. The slurry was dried and subsequently calcined at 850 °C for 6 h. The calcined powders were milled and dried again, and then were pressed into disks with a diameter of about 10 mm and a thickness of about 1.0 mm under a uniaxial pressure of 10 MPa after using the 3–5 wt% polyvinyl alcohol (PVA) as a binder. After burning off the PVA at 500 °C for 2 h, all the pellets were sintered at 1150 °C for 3 h in air, except those with the composition $x = 0$, which were sintered at 1110 °C.

An X-ray diffractometer (XRD) (XRD-6100, Shimadzu, Japan) was used to analyze the phase structures of these sintered ceramic samples, and their microstructures were observed using a scanning electron microscope (SEM) (JSM-6610, JEOL, Japan), equipped with an energy dispersive spectrometer that was used to analyze the chemical composition. The densities of the sintered samples were determined by the Archimedes water immersion method. In order to characterize the electrical properties of the ceramics, the silver paste was coated on both sides of them and
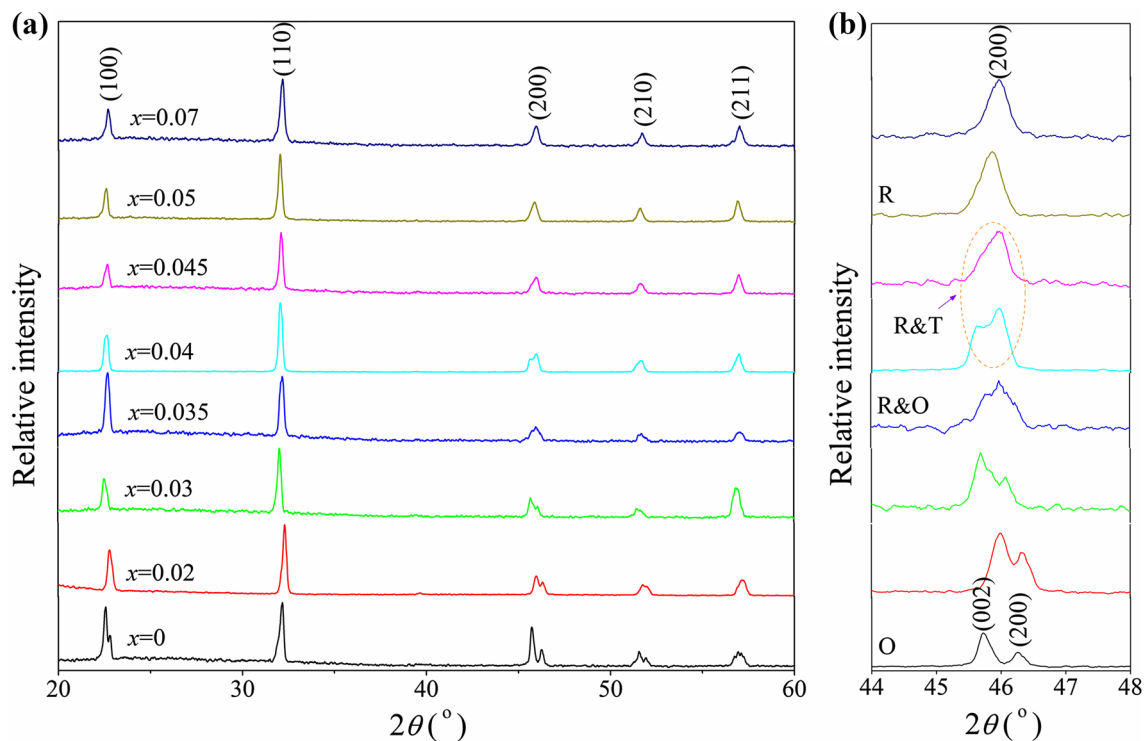

Fig. 1 XRD patterns of the KNN-CZ-xBNH ceramics in the 2θ range of **a** 20–60° and **b** 44–48°

then fired at 650 °C for 10 min. The temperature-dependent dielectric properties were measured via a computer-controlled precision LCR meter (E4980A, Keysight Technologies, USA). For piezoelectric characterization, the samples were poled at 40 °C in a silicone oil bath by applying a DC electric field of 3–4 kV/mm for 30 min. After aging for 24 h, the piezoelectric constant d_{33} was measured on a quasi-static d_{33} meter (YE2730A, Wuxi Yutian, China). A resonance–antiresonance method was employed to determine the planar electromechanical coupling coefficients (k_p) of the ceramics using an impedance analyzer (E4990A, Keysight Technologies, USA) on the basis of IEEE standards.

3 Results and discussion

Figure 1a shows the XRD patterns of the KNN–CZ–xBNH ceramics, measured at room temperature and in the 2θ range

of 20–60°. It can be observed that all the samples possess a single perovskite structure, indicating that the BNH has a good solubility in the KNN-based solid solutions. The good solubility between the BNH dopant and the KNN–CZ host can be further verified by the uniform elemental distribution in the ceramics, as show in Fig. 2, which was obtained using an energy dispersive X-ray analyzer (EDAX).

For better identification of the structural evolution of the ceramics, the enlarged XRD patterns are shown in Fig. 1b, with the 2θ range of 44–48°. It is notable that the ceramics with compositions $x \leq 0.03$ have an orthorhombic symmetry, as they show split peaks at about 46°, respectively identified as (200) and (002), and the two peaks have an intensity ratio (I_{200}/I_{002}) of about 1:2, which is a typical characteristic of orthorhombic phase in KNN-based ceramics [28]. Moreover, one can observe that the split peaks merge into a single one for the ceramics with the compositions of $x \geq 0.05$, suggesting that they possess a rhombohedral
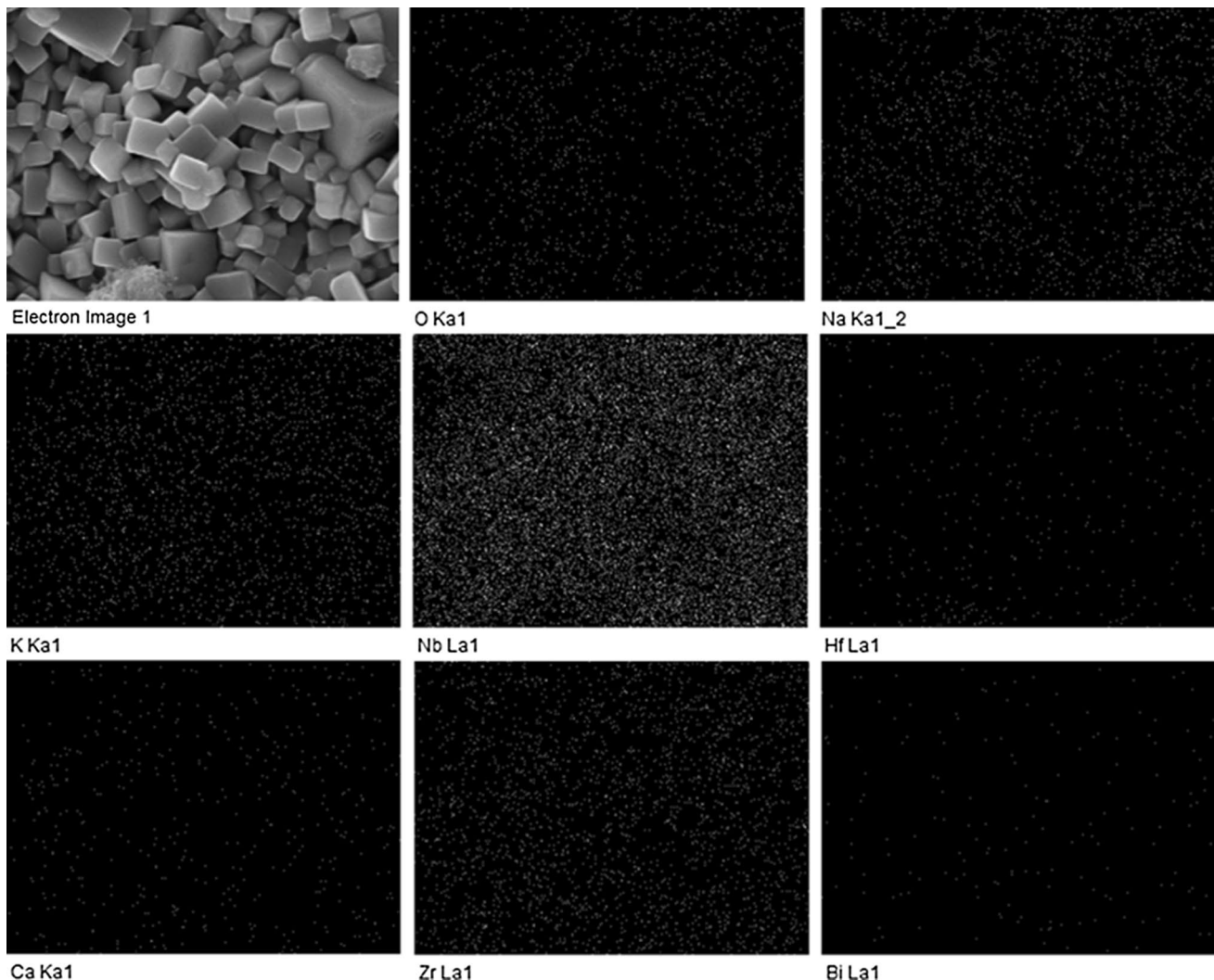

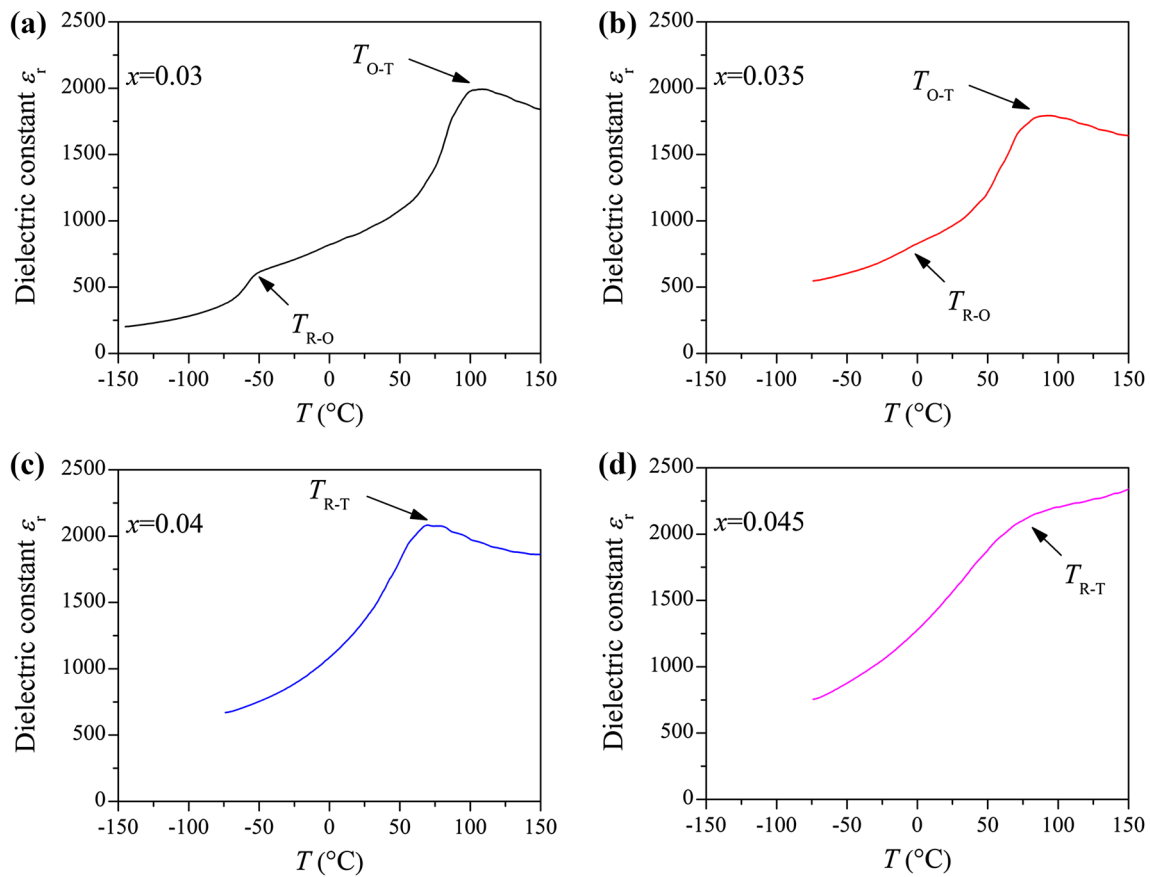**Fig. 2** Elemental mapping of the KNN–CZ–xBNH ceramics with $x = 0.04$

Fig. 3 Dielectric-temperature curves of the KNN–CZ–xBNH ceramics in the temperature range from about − 150 to 150 °C

structure. Nevertheless, the ceramics with compositions $0.035 \leq x \leq 0.045$ could not be identified as any phase only given the XRD results. Therefore, for more detailed structural analysis, it is necessary to combine the XRD patterns with other experimental data, such as dielectric-temperature curves, as displayed in Fig. 3.

The dielectric-temperature curves in Fig. 3 were measured at a frequency of 10 kHz and in the temperature range of about − 150 to 150 °C. For the ceramics with compositions $x \leq 0.035$, two dielectric anomalies, corresponding to the R–O and O–T phase transitions respectively, can be observed in the curves. It is clearly evident that the addition of BNH simultaneously shifts both the temperatures of the two phase transitions (i.e., the T_{R-O} and T_{O-T}) to room temperature, which is beneficial for the formation of R–T phase boundary, as pointed out previously. For the composition $x = 0.035$, its T_{R-O} is near room temperature, while its T_{O-T} is far above room temperature, indicating it has an R–O phase boundary at room temperature. With the further increase of BNH content, the two temperatures converge at $0.04 \leq x \leq 0.045$. The convergence of the two temperatures is important evidence that the R–T boundary has been

formed, as suggested by many references [7, 23–25]. Therefore, according to these results together with the previous XRD analysis, one can reasonably conclude that the ceramics possess an R–T phase boundary in the composition range of $0.04 \leq x \leq 0.045$.

Figure 4 displays the SEM micrographs of the KNN–CZ–xBNH ceramics with $x = 0$, 0.02, 0.03, 0.04, and 0.05. It can be seen that the grains of the ceramics become extremely large with the addition of a small amount of BNH. The extreme growth of grains can be ascribed to the high sintering temperature, but in this work, it is the added Bi^{3+} and Hf^{4+} cations, which respectively occupy the A and B sites of the ABO_3 perovskite structure, that provide the most important contributions to the extremely large grain sizes. This is because the introduction of Bi^{3+} and Hf^{4+} ions, which have valences different from those of other cations, may produce a large amount of B-site and oxygen vacancies, respectively, in the crystal lattices [26, 27]. And as is well-known, the vacancies always promote the grain growth during the sintering of ceramics. However, when the amount of added BNH exceeds a certain value, many Bi^{3+} and Hf^{4+} ions will aggregate at the grain boundaries [28], which can hinder
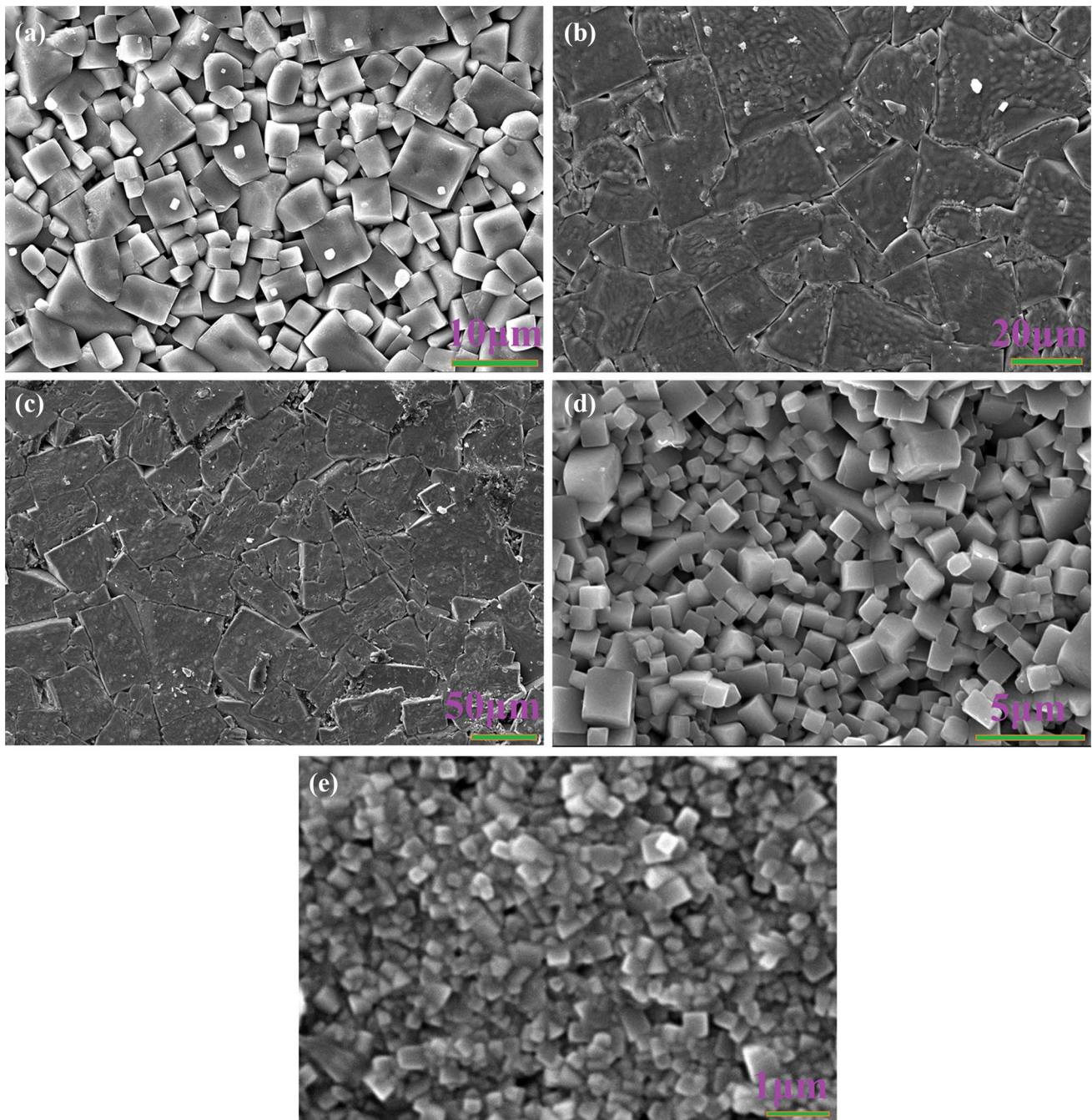
Fig. 4 SEM micrographs of the KNN–CZ–xBNH ceramics for **a** $x=0$, **b** $x=0.02$, **c** $x=0.03$, **d** $x=0.04$, and **e** $x=0.05$

grain growth and thereby leads to smaller grain sizes in the materials, as shown in Fig. 4d, e. Particularly in Fig. 4e, an extremely fine grain size is observed for the ceramics with the composition $x=0.05$. This means that adding too much BNH will result in a lower sintering activity in the KNN-based ceramics, which generally has adverse effects on the electrical properties.

For further evaluating the quality of the sintered samples, the densities of the KNN–CZ–xBNH ceramics have been measured, as illustrated in Fig. 5. It can be found that the density shows an increasing trend with the addition of BNH until $x=0.045$, above which the density begins to decrease upon further increasing the BNH content. Apparently, it is the degradation in sintering activity (as discussed previously) that leads to the reduced density for the ceramics with relatively high BNH contents.

To identify the effects of BNH content on the ferro-paraelectric phase transition, the dielectric constants of the
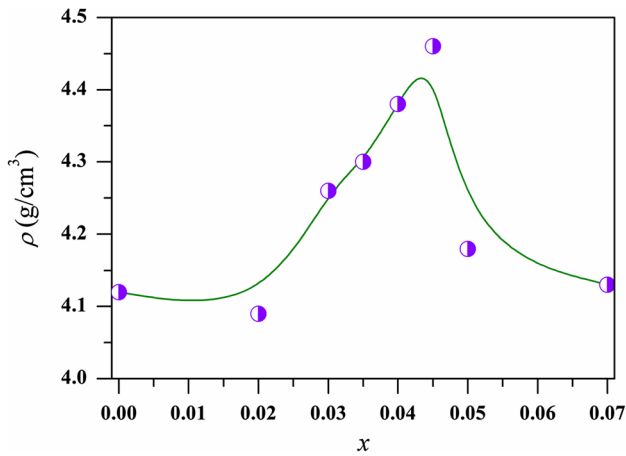
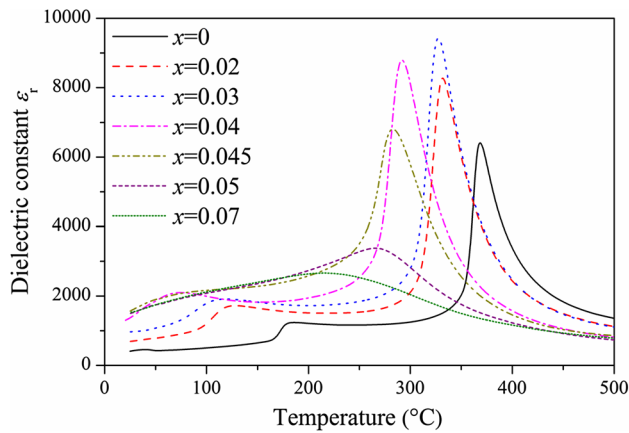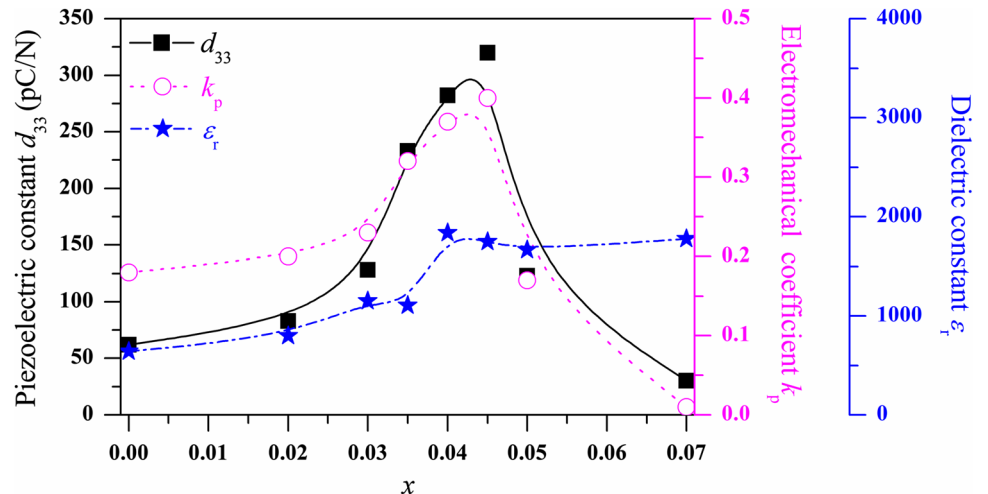**Fig. 5** Density of the KNN–CZ–xBNH ceramics as a function of BNH content

Fig. 6 Dielectric-temperature curves of the KNN–CZ–xBNH ceramics in the temperature range from room temperature to 500 °C

KNN–CZ–xBNH ceramics were measured from room temperature to 500 °C, as shown in Fig. 6. It can be observed that the temperature of the Curie peak (approximately determined as T_C) gradually declines as x increases. Furthermore, a sharp Curie peak can be seen for the ceramics with the compositions of $x \leq 0.04$. However, when $x \geq 0.045$, the Curie peak tends to broaden upon the further increase of BNH content, and eventually develops into a very broad and flat shape for the compositions $x \geq 0.05$, exhibiting features of diffuse phase transition. This should be attributed to the inhomogeneous distribution of various cations at A and B sites of the pervoskite structure [29], which is rather difficult to be avoided due to the phase segregation of end members over a wide temperature interval, as suggested by Refs. [30, 31].

Figure 7 illustrates the piezoelectric constant d_{33}, planar electromechanical coupling coefficient (k_p), and relative dielectric constant ε_r (measured at 1 kHz) of the KNN–CZ–xBNH ceramics as functions of x. It can be found that both the d_{33} and k_p firstly rise and then decrease alongside the increase of BNH content, and that they reach their respective maximum values of 320 pC/N and 0.40 at $x = 0.045$. The enhanced piezoelectric activity should be attributed to the R–T phase boundary that causes the lower energy barrier for polarization rotation, due to the involvement of more polarization states [1, 32]. However, as the crystal structure becomes a sole rhombohedral phase at $x = 0.05$, the ceramics experience a dramatic reduction in both the d_{33} and k_p. Moreover, one can see that the ε_r tends to increase with x, in spite of a slight enhancement appearing at the R–T phase boundary. A similar tendency of increase in ε_r with the amount of BNH has been found in other BNH-modified KNN-based ceramics as well [33]. To sum up, our results suggest that the addition of BNH is an effective method for the construction of R–T phase boundaries as well

Fig. 7 d_{33}, k_p, and ε_r of the KNN–CZ–xBNH ceramics as functions of BNH content

as the improvement of electrical properties in KNN-based ceramics.

4 Conclusion

Lead-free KNN–CZ–xBNH piezoelectric ceramics were fabricated by a conventional solid-state reaction method. In the studied composition range, all the ceramics possess a single perovskite structure, without any detectable secondary phase. The ceramics possess an R–T phase boundary in the composition range of $0.04 \leq x \leq 0.045$, near which the materials exhibit enhanced piezoelectric activity, with maximum values of d_{33} and k_p, being 320 pC/N and 0.40 respectively. The formation of the R–T phase boundary is due to the fact that the introduction of BNH can simultaneously shift both the $T_{R–O}$ and $T_{O–T}$ to room temperature. Furthermore, the addition of a small amount of BNH can promote the grain growth of the ceramics during the sintering process, and even may result in extremely large grain sizes. Overall, our results suggest that the addition of BNH is an effective means for the construction of R–T phase boundaries in KNN-based ceramics, which can lead to a significant enhancement of piezoelectric properties.

References

1. B. Jaffe, W.R. Cook Jr., H. Jaffe, *Piezoelectric Ceramics* (Academic Press, New York, 1971)
2. G.H. Haertling, Ferroelectric ceramics: history and technology. J. Am. Ceram. Soc. **82**, 797–818 (1999)
3. P.K. Panda, Review: environmental friendly lead-free piezoelectric materials. J. Mater. Sci. **44**, 5049–5062 (2009)
4. J. Rödel, W. Jo, K.T.P. Seifert, E.M. Anton, T. Granzow, D. Damjanovic, Perspective on the development of lead-free piezoceramics. J. Am. Ceram. Soc. **92**, 1153–1177 (2009)
5. T.R. Shrout, S.J. Zhang, Lead-free piezoelectric ceramics: alternatives for PZT. J. Electroceram. **19**, 111–124 (2007)
6. T. Zheng, W.J. Wu, J.G. Wu, J.G. Zhu, D.Q. Xiao, Balanced development of piezoelectricity, Curie temperature, and temperature stability in potassium–sodium niobhrate lead-free ceramics. J. Mater. Chem. C **4**, 9779–9787 (2016)
7. J.G. Wu, D.Q. Xiao, J.G. Zhu, Potassium–sodium niobate lead-free piezoelectric materials: past, present, and future of phase boundaries. Chem. Rev. **115**, 2559–2595 (2015)
8. J.G. Wu, D.Q. Xiao, J.G. Zhu, Potassium–sodium niobate lead-free piezoelectric ceramics: recent advances and perspectives. J. Mater. Sci.: Mater. Electron. **26**, 9297–9308 (2015)
9. J.F. Li, K. Wang, F.Y. Zhu, L.Q. Cheng, F.Z. Yao, (K,Na)NbO$_3$-based lead-free piezoceramics: fundamental aspects, processing technologies, and remaining challenges. J. Am. Ceram. Soc. **96**, 3677–3696 (2013)
10. Y. Saito, H. Takao, T. Tani, T. Nonoyama, K. Takatori, T. Homma, T. Nagaya, M. Nakamura, Lead-free piezoceramics. Nature **432**, 84–87 (2004)
11. J. Yin, J.G. Wu, H. Wang, Composition dependence of electrical properties in (1 − x)KNbO3–xNaNbO$_3$ lead-free ceramics. J. Mater. Sci.: Mater. Electron. **28**, 4828–4838 (2017)
12. K.P. Chen, F.L. Zhang, D.S. Li, J. Tang, Y.L. Jiao, L.N. An, Acceptor doping effects in (K$_{0.5}$Na$_{0.5}$)NbO$_3$ lead-free piezoelectric ceramics. Ceram. Int. **42**, 2899–2903 (2016)
13. R.A. Bucur, I. Badea, A.I. Bucur, S. Novaconi, Dielectric, ferroelectric and piezoelectric proprieties of GdCoO$_3$ doped (K$_{0.5}$Na$_{0.5}$)NbO$_3$. J. Alloys Compd. **630**, 43–47 (2015)
14. Y. Chen, D.D. Xue, P. Wang, X.Q. Jiang, Z.Q. Chen, X.K. Liu, G. Liu, Z.P. Xu, Lead-free K$_{0.5}$Na$_{0.5}$NbO$_3$–Bi$_{0.5}$Li$_{0.5}$ZrO$_3$–BiAlO$_3$ ternary ceramics: structure and piezoelectric properties. J. Electroceram. (2017). doi:10.1007/s10832-017-0089-7
15. L.M. Jiang, Y.Y. Li, L.X. Xie, J.G. Wu, Q. Chen, W. Zhang, D.Q. Xiao, J.G. Zhu, Enhanced electrical properties and good thermal stability in K$_{0.48}$Na$_{0.52}$NbO$_3$–LiNbO$_3$–BiAlO$_3$ lead-free piezoceramics. J. Mater. Sci.: Mater. Electron. **28**, 8500–8509 (2017)
16. D.D. Xue, M. Shi, Y. Chen, K.H. Liu, Z.Q. Chen, X.Q. Jiang, Piezoelectric and dielectric properties of lead-free 0.96(K$_{0.48}$Na$_{0.535}$)$_{0.96}$Li$_{0.04}$Nb$_{1−x}$Sb$_x$O$_3$–0.04CaZrO$_3$ ceramics with rhombohedral–orthorhombic phase boundary. Ferroelectrics **514**, 1–8 (2017)
17. F.L. Li, Z. Tan, J. Xing, L.M. Jiang, B. Wu, J.G. Wu, D.Q. Xiao, J.G. Zhu, Investigation of new lead free (1−x)KNNS–xBKZH piezoceramics with R–O–T phase boundary. J. Mater. Sci.: Mater. Electron. **28**, 8803–8809 (2017)
18. Y. Chen, D.D. Xue, Z.Q. Chen, X.Q. Jiang, J. Gou, G. Liu, X.K. Liu, Z.P. Xu, Lithium-modified (K$_{0.5}$Na$_{0.5}$)NbO$_3$–BiAlO$_3$ lead-free piezoelectric ceramics with high Curie temperature. Ceram. Int. **43**, 634–640 (2017)
19. Z. Tan, J. Xing, B. Wu, J.G. Wu, J.G. Zhu, D.Q. Xiao, Novel rhombohedral and tetragonal phase boundary with high T_C in alkali niobate ceramics. J. Mater. Sci.: Mater. Electron. **28**, 12851–12857 (2017)
20. Y. Chen, D.D. Xue, Y. Ma, Z.Q. Chen, X.Q. Jiang, G. Liu, X.K. Liu, Piezoelectric and dielectric properties of 0.995K$_{0.48}$Na$_{0.48}$Li$_{0.04}$Nb$_{(1−x)}$Sb$_x$O$_3$–0.005BiAlO$_3$ lead-free piezoelectric ceramics. Mater. Res. Bull. **84**, 240–244 (2016)
21. X. Lv, J.G. Wu, S. Yang, D.Q. Xiao, J.G. Zhu, Identification of phase boundaries and electrical properties in ternary potassium-sodium niobate-based ceramics. ACS Appl. Mater. Interfaces **8**, 18943–18953 (2016)
22. Y. Chen, D.D. Xue, Y. Ma, K.H. Liu, Z.Q. Chen, X.Q. Jiang, Phase transitional behavior and electrical properties of (1−x)(K$_{0.475}$Na$_{0.48}$Li$_{0.05}$)Nb$_{0.95}$Sb$_{0.05}$O$_3$–xCaZrO$_3$ lead-free ceramics. Phys. Lett. A **380**, 2974–2978 (2016)
23. T. Zheng, H.J. Wu, Y. Yuan, X. Lv, Q. Li, T.L. Men, C.L. Zhao, D.Q. Xiao, J.G. Wu, K. Wang, J.F. Li, Y.L. Gu, J.G. Zhu, S.J. Pennycook, The structural origin of enhanced piezoelectric performance and stability in lead free ceramics. Energy Environ. Sci. **10**, 528–537 (2017)
24. B. Wu, H.J. Wu, J.G. Wu, D.Q. Xiao, J.G. Zhu, S.J. Pennycook, Giant piezoelectricity and high Curie temperature in nanostructured alkali niobate lead-free piezoceramics through phase coexistence. J. Am. Chem. Soc. **138**, 15459–15464 (2016)
25. K. Xu, J. Li, X. Lv, J.G. Wu, X.X. Zhang, D.Q. Xiao, J.G. Zhu, Superior piezoelectric properties in potassium–sodium niobate lead-free ceramics. Adv. Mater. **28**, 8519–8523 (2016)

26. Y. Chen, D.D. Xue, M. Shi, X.Q. Jiang, Z.Q. Chen, X.K. Liu, G. Liu, Z.P. Xu, Effects of $Bi_{0.5}Na_{0.5}HfO_3$ addition on the phase structure and piezoelectric properties of $(K,Na)NbO_3$–based ceramics. J. Am. Ceram. Soc. **100**, 3920–3927 (2017)

27. H. Tao, J.G. Wu, Giant piezoelectric effect and high strain response in $(1-x)(K0.45Na0.55)(Nb1-ySby)O3-xBi0.5Na0.5Zr1-zHfzO3$ lead-free ceramics. J. Eur. Ceram. Soc. **36**, 1605–1612 (2016)

28. X. Lv, Z.Y. Li, J.G. Wu, J.W. Xi, M. Gong, D.Q. Xiao, J.G. Zhu, Enhanced piezoelectric properties in potassium-sodium niobate-based ternary ceramics. Mater. Des. **109**, 609–614 (2016)

29. A. Munpakdee, K. Pengpat, J. Tontrakoon, T. Tunkasiri, The study of dielectric diffuseness in the $Ba(Mg_{1/3}Nb_{2/3})O_3$–$BaTiO_3$ ceramic system. Smart Mater. Struct. **15**, 1255–1259 (2006)

30. L. Ramajo, M. Castro, A. del Campo, J.F. Fernandez, F. Rubio-Marcos, Revealing the role of cationic displacement in potassium–sodium niobate lead-free piezoceramics by adding W^{6+} ions. J. Mater. Chem. C **3**, 4168–4178 (2015)

31. J. Venkatesh, V. Sherman, N. Setter, Synthesis and dielectric characterization of potassium niobate tantalate ceramics. J. Am. Ceram. Soc. **88**, 3397–3404 (2005)

32. W.F. Liu, X.B. Ren, Large piezoelectric effect in Pb-free ceramics. Phys. Rev. Lett. **103**, 257602 (2009)

33. H. Tao, J.G. Wu, T. Zheng, X.J. Wang, X.J. Lou, New $(1-x)$ $K_{0.45}Na_{0.55}Nb_{0.96}Sb_{0.04}O_3$–$xBi_{0.5}Na_{0.5}HfO_3$ lead-free ceramics: phase boundary and their electrical properties. J. Appl. Phys. **118**, 044102 (2015)